

Article

Effect of CaO Sourced from CaCO₃ or CaSO₄ on Phase Formation and Mineral Composition of Iron-Rich Calcium Sulfoaluminate Clinker

Wen Jiang¹, Changliang Wu¹, Chao Zhang¹, Xujiang Wang^{1,*}, Yuzhong Li¹, Shuang Wu², Yonggang Yao¹, Jingwei Li^{1,*}  and Wenlong Wang^{1,*}

¹ National Engineering Laboratory for Reducing Emissions from Coal Combustion, Engineering Research Center of Environmental Thermal Technology, Ministry of Education, Shandong Key Laboratory of Energy Carbon Reduction and Resource Utilization, School of Energy and Power Engineering, Shandong University, Jinan 250061, China

² School of Mechanical Engineering, Tianjin University of Commerce, Tianjin 300134, China

* Correspondence: x.wang@sdu.edu.cn (X.W.); ljw@sdu.edu.cn (J.L.); wwenlong@sdu.edu.cn (W.W.)

Abstract: The performance of iron-rich calcium sulfoaluminate (IR-CSA) cement is greatly affected by mineral composition and mineral activity in the clinker. This study aims to identify the effect of CaO sources, either CaCO₃ or CaSO₄, on the phase formation and mineral composition of the IR-CSA clinker. Targeted samples were prepared with different proportions of CaCO₃ and CaSO₄ as CaO sources at 1300 °C for 45 min. Multiple methods were used to identify the mineralogical conditions. The results indicate that the mineral composition and performance of the IR-CSA clinker could be optimized by adjusting the CaO source. Both Al₂O₃ and Fe₂O₃ tend to incorporate into C₄A_{3-x}F_xS̄ with an increase in CaSO₄ as a CaO source, which leads to an increased content of C₄A_{3-x}F_xS̄ but a decreased ferrite phase. In addition, clinkers prepared with CaSO₄ as a CaO source showed much higher *x* value in C₄A_{3-x}F_xS̄ and higher compressive strength than clinker prepared with CaCO₃ as the sole CaO source. The crystal types of both C₄A_{3-x}F_xS̄ and C₂S were also affected, but showed different trends with the transition of the CaO source. The findings provide a possible method to produce IR-CSA cement at a low cost through cooperative utilization of waste gypsum and iron-bearing industrial solid wastes.

Keywords: phase formation; mineral composition; iron-bearing ye'elimite; incorporation



Citation: Jiang, W.; Wu, C.; Zhang, C.; Wang, X.; Li, Y.; Wu, S.; Yao, Y.; Li, J.; Wang, W. Effect of CaO Sourced from CaCO₃ or CaSO₄ on Phase Formation and Mineral Composition of Iron-Rich Calcium Sulfoaluminate Clinker. *Materials* **2023**, *16*, 643. <https://doi.org/10.3390/ma16020643>

Academic Editor: Giuseppe Cruciani

Received: 19 November 2022

Revised: 5 January 2023

Accepted: 6 January 2023

Published: 9 January 2023



Copyright: © 2023 by the authors. Licensee MDPI, Basel, Switzerland. This article is an open access article distributed under the terms and conditions of the Creative Commons Attribution (CC BY) license (<https://creativecommons.org/licenses/by/4.0/>).

1. Introduction

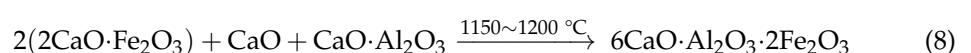
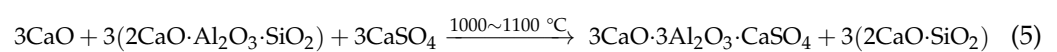
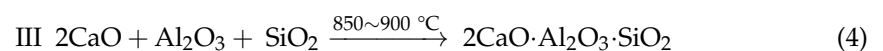
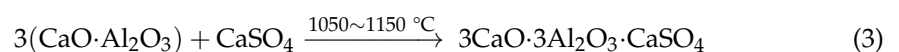
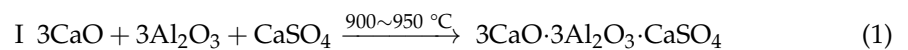
Calcium sulfoaluminate (CSA) cement, which was first developed in China 40 years ago, has attracted increasing attention due to its lower energy consumption and CO₂ emissions than Portland cement (PC) [1–3]. CSA clinker consists mainly of calcium sulfoaluminate (C₄A₃S̄), dicalcium silicate (C₂S), and ferrite phases (C₂F~C₆A₂F). It can be produced at 1200 °C–1300 °C, which is about 150 °C lower than PC clinker production [4]. CSA cement exhibits excellent performance in engineering construction, such as precast products, 3D printing, marine-engineering concrete and cold environments, due to its characteristics of high early-age strength, rapid setting, low permeability, and low alkalinity [5–8]. Therefore, CSA cement will be a promising alternative to PC in future.

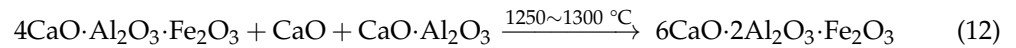
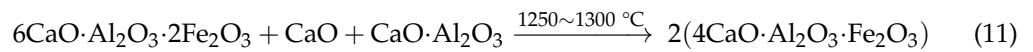
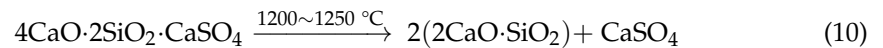
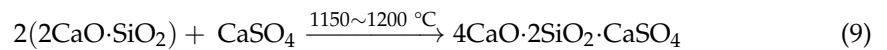
The high cost of raw meal has limited the massive scale application of CSA cement in engineering construction, especially expensive bauxite. To reduce production costs, CSA has been produced by using industrial solid wastes (ISWs) containing aluminum, such as aluminum ash and red mud, instead of high-grade bauxite [4,7–9]. However, aluminum-bearing ISWs such as red mud, steel slag, and tailings are rich in iron. The presence of iron has an impact on the formation, composition, and hydration activity of the key mineral phases in CSA clinker [10–13]. Iron is reported mainly to transform to the ferrite phase

and ye'elimite [14] and that will make difference to the cement performance. The ferrite phase is beneficial to the early strength, but the ye'elimite is beneficial to both the early and late compressive strength [15,16]. More importantly, the incorporation of iron into ye'elimite makes it possible to decrease the aluminum content in raw materials and expand the aluminum sources. Therefore, researchers have tried to introduce more Fe_2O_3 into $\text{C}_4\text{A}_{3-x}\text{F}_x\bar{\text{S}}$ in iron-rich calcium sulfoaluminate (IR-CSA) clinker.

Several researchers produced IR-CSA clinker in $\text{CaO-SiO}_2\text{-Al}_2\text{O}_3\text{-Fe}_2\text{O}_3\text{-SO}_3$ -based systems and found that the x value in $\text{C}_4\text{A}_{3-x}\text{F}_x\bar{\text{S}}$ is greatly affected by the Fe_2O_3 , SO_3 , and CaO proportions in the raw mixture [14,17–19]. Studies have confirmed that the x value in $\text{C}_4\text{A}_{3-x}\text{F}_x\bar{\text{S}}$ presents a rising trend with the increase in Fe_2O_3 content in the raw material; however, not all Fe_2O_3 can be substituted for Al_2O_3 to participate in the formation of $\text{C}_4\text{A}_{3-x}\text{F}_x\bar{\text{S}}$ [18]. Low CaO and rich SO_3 content in raw mixtures have also proven effective in promoting the incorporation of Fe_2O_3 into $\text{C}_4\text{A}_{3-x}\text{F}_x\bar{\text{S}}$ in calcium sulphaluminate ferrite-based systems [17,19]. It is obvious that both CaO and SO_3 could be provided by CaSO_4 . Thus, it is feasible to ensure sufficient SO_3 by batching excessive CaSO_4 as CaO sources in the raw material.

CaO is derived from both CaCO_3 and CaSO_4 during the sintering process. Some researchers have indicated that the content of CaSO_4 as a CaO source has an influence on the mineral composition of the clinker and further affects the performance of the cement. They have reported that a small amount of CaSO_4 as a CaO source makes no obvious difference to the mineral composition of the clinker and that the loss of SO_3 was compensated to promote adequate formation of ye'elimite; however, excess CaSO_4 as a CaO source was reported to lead to the formation of gehlenite, thereby decreasing the compressive strength of the cement [20,21]. Others have indicated that CSA clinker could be obtained with CaO as provided by the partial decomposition of CaSO_4 , with both the key mineral phase composition of the clinker and the properties of the cement being similar to that produced by traditional methods (CaO source from CaCO_3) [22]. In particular, CSA clinker with CaSO_4 as the entire CaO source was produced with adequate formation of key mineral phases [23]. In our previous study, we found that batching the slight excess of CaSO_4 in the raw mixture is an effective method of promoting the utilization rate of Al_2O_3 (to form $\text{C}_4\text{A}_{3-x}\text{F}_x\bar{\text{S}}$) [17,20]. In addition, the crystal structure of ye'elimite transformed from orthorhombic symmetry to cubic symmetry because of the incorporation of Fe_2O_3 , and the x value of $\text{C}_4\text{A}_{3-x}\text{F}_x\bar{\text{S}}$ increased with the increase in CaSO_4 content. We also prepared IR-CSA with gypsum as the entire CaO source and found that the added iron did not form the ferrite phase first but was incorporated into other phases such as ye'elimite [14]. From the above studies, we found that the phase formation, transformation, and composition of IR-CSA clinker is greatly affected by CaO sources. However, the conclusions of the above studies are slightly biased due to the different preparation conditions. Systematic research into the effect of CaO sources on the phase formation and mineralogic conditions of IR-CSA clinker are still limited, and the mechanism remains unclear.





To make clear the effect of the CaO source, as either CaCO₃/limestone or CaSO₄/gypsum, on the mineralogic conditions of IR-CSA clinker, the targeted clinker was prepared with the mineral proportion of C₄A₃S̄:C₂S:C₄AF as 50:30:20 by mass. Five groups of raw materials with increasing proportions of CaSO₄ as a CaO source were designed; namely, whole CaCO₃ (the CaSO₄ was assumed to be undecomposed), 90 at.% CaCO₃ + 10 at.% CaSO₄ (at.% is the abbreviation form of the atomic ratio in the text), 80 at.% CaCO₃ + 20 at.% CaSO₄, 50 at.% CaCO₃ + 50 at.% CaSO₄, 20 at.% CaCO₃ + 80 at.% CaSO₄ and 100 at.% CaSO₄ were designed to produce the clinkers. To ensure that the mineral formation was complete, all clinker was prepared at 1300 °C for 45 min. The mineralogic conditions as well as the microstructure and the chemical composition of key minerals, which would be influenced by the CaO source, were identified by multiple methods. Finally, the compressive strength was tested as a supplemental validation to verify the feasibility of optimizing the mineralogic conditions of the IR-CSA clinker and further the performance of the IR-CSA cement by adjusting the content of CaSO₄ as the CaO source.

2. Materials and Methods

2.1. Raw Mixture

The raw materials (CaCO₃, Al₂O₃, CaSO₄·2H₂O, Fe₂O₃, and SiO₂) for preparing the IR clinker were analytical reagents provided by the Sinopharm Group Chemical Reagent Co., Ltd., Shanghai, China. CaCO₃ was used as the CaO source. CaSO₄ provided both CaO and SO₃ during the calcination process of the IR-CSA clinker.

The targeted mineral composition of all clinker and the contents of the raw materials in the preparation of 100 g clinker with chemical reagents are shown in Table 1. The Bogue method was used to obtain the corresponding raw mixture [17]. The clinkers were named as S00, S10, S20, S50, S80, and S100, based on the content of CaO in the form of CaSO₄. C_m indicates the degree of CaO in the raw material in order to satisfy that required for the formation of useful minerals in the corresponding clinker. The formula of C_m is defined as in Equation (13), and the value is fixed as 1.00 in this study. The Fe₂O₃/(Al₂O₃ + Fe₂O₃) ratio was the same for all the clinker in this study.

$$C_m = \frac{w(\text{CaO}) - 0.7w(\text{TiO}_2)}{0.73[w(\text{Al}_2\text{O}_3) - 0.64w(\text{Fe}_2\text{O}_3)] + 1.4w(\text{Fe}_2\text{O}_3) + 1.87w(\text{SiO}_2)} \quad (13)$$

Table 1. Target mineral composition of the clinker and chemical reagent proportions in the raw materials to prepare 100 g clinker.

Sample	Targeted Minerals				Raw Material Proportion			
	C ₄ A ₃ S̄	C ₂ S	C ₄ AF	CaCO ₃	SiO ₂	Al ₂ O ₃	Fe ₂ O ₃	CaSO ₄ ·2H ₂ O
S00	50	30	20	55.69	7.67	21.47	4.83	10.34
S10	50	30	20	48.19	7.37	20.64	4.64	19.15
S20	50	30	20	41.25	7.10	19.88	4.47	27.31
S50	50	30	20	23.20	6.39	17.89	4.02	48.51
S80	50	30	20	8.43	5.81	16.26	3.65	65.85
S100	50	30	20	0	5.47	15.33	3.44	75.76

2.2. Preparation Method

The reagents were dried at 110 °C for 2 h in a muffle furnace (LYL-16MA, LUO YANG LIYU KILN CO., LTD, Luoyang, China) and were then ground together in an agate bowl for 1 h to ensure the homogenization of the raw mixture; alcohol was added as a dispersant in the grind progress. After homogenization, 50 g per sample of raw mixture was added to the stainless steel mold (Tianjin Jingtuo Instrument Technology Co., LTD, Tianjin, China); a columnlike raw mixture with a 35 mm diameter was obtained under a pressure of 20 MPa. Thereafter, the obtained columnlike raw mixtures were fired in an elevator-hearth furnace (LYL-17SJ, LUOYANG LIYU KILN CO., LTD, Luoyang, China) at 1300 °C for 45 min and then rapidly cooled at room temperature. Finally, the IR-CSA cement was obtained by milling the clinkers and gypsum. The gypsum added to the clinkers to react with ye'elimite would promote the formation of $C_6A\bar{S}_3H_{32}$ (AFt) according to Equation (14), but samples with higher M ratios hydrated too fast to form cracks between AFt [24] and thus decreased the mechanical properties of the cement. The optimal gypsum content mixed with clinkers were samples with 0.8 m ratios of gypsum- (the anhydrate in clinkers was involved) to-ye'elimite (M) suggested by [10] and [25]. The content of ye'elimite and anhydrate were determined by the Rietveld refinement method [26]. Subsequently, the cement was prepared as cubic specimens (20 mm × 20 mm × 20 mm) with the water-to-cement ratio of 0.28.



where $C_4A_3\bar{S}$, $C\bar{S}H_x$ and $C_6A\bar{S}_3H_{32}$ are the abbreviated form of $3CaO \cdot Al_2O_3 \cdot CaSO_4$, $CaSO_4 \cdot xH_2O$ and $6CaO \cdot Al_2O_3 \cdot SO_3 \cdot 32H_2O$, respectively, and the superscript on S represents sulfate in the compound.

2.3. Testing Methods

The phenyl formic acid–ethyl alcohol titration method was adopted to determine the f-CaO content of the IR-CSA clinker according to the Chinese standard GB/T 176–2017.

The sulfate loss was calculated according to the difference in the SO_3 amount between the raw materials and the clinkers. The SO_3 contents were determined according to the barium sulfate precipitation in accordance with the Chinese standard GB/T176–2008 [23]. The gypsum decomposition rate is expressed as follows:

$$\text{Decomposition rate (\%)} = \frac{M_1 \times S_1 - M_2 \times S_2}{M_1 \times S_1} \quad (15)$$

where M_1 and S_1 represent the mass and SO_3 content of a raw sample, respectively; M_2 and S_2 are the mass and SO_3 content of a clinker sample, respectively.

The mineral phase assemblages of all clinkers were determined by an X-ray diffractometer (Aeris, Malvern Panalytical, Malverin, UK) with Cu-K α radiation. The voltage and the current were set to 40 KV and 15 mA, respectively. The detection range of the X-ray diffraction spectra was set to 10–60° with a scanning speed of 0.0027° per step. The mineral composition was quantified by Rietveld refinement using Topas-Academic V6 software. The crystallographic structures of the phases involved are listed in Table 2. The refined parameters included the background coefficients, instrument parameters, zero-shift error and unit cell parameters [14].

The microstructure of the pattern was acquired by scanning electron microscopy (SEM, Quattro S, Thermo Fisher Scientific, Waltham, MA, USA) with an acceleration voltage of 5 kV.

The chemical composition of clinkers was obtained by a field emission electron probe (FE-EPMA, JXA-8530F-Plus, Tokyo, Japan), and the backscattered electron (BSE) images and elemental distribution images of the patterns were detected with an acceleration voltage of 15 KV and an electron beam current of 5×10^{-8} A. The samples were first completely covered with epoxy resin and polished to a mirror state; the prepared patterns were then sprayed with carbon to improve their electrical conductivity for microanalysis.

Table 2. Crystallographic structures and ICSD codes of phases involved in the Rietveld refinement.

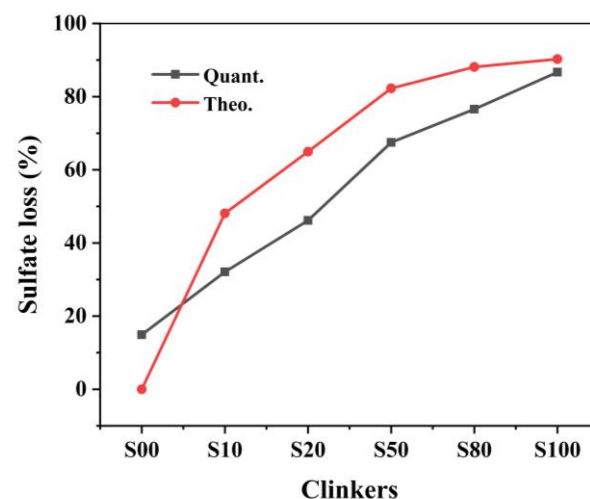
Scientific Names	Crystal System	Space Group	Abbrev. of Formula	Chemical Formula	ICSD
Ye'elimite- <i>c</i>	cubic	I-43m	$C_4A_3\bar{S}$ -c	$Ca_4Al_6SO_{16}$	9560
Ye'elimite- <i>o</i>	orthorhombic	Pcc2	$C_4A_3\bar{S}$ -o	$Ca_4Al_6SO_{16}$	80,361
Belite-beta	Monoclinic	P21/ <i>n</i>	C_2S -beta	Ca_2SiO_4	79,550
Belite-al'	orthorhombic	Pnma	C_2S -al'	Ca_2SiO_4	81,097
Srebrodolskite	orthorhombic	Pnma	C_2F	$Ca_2Fe_2O_5$	15,059
Brownmillerite	orthorhombic	Ibm2	C_4AF	$Ca_4Al_2Fe_2O_{10}$	9197
Gehlenite	Tetragonal	<i>p</i> -421m	C_2AS	$Ca_2Al_2SiO_7$	87,144
Anhydrite	orthorhombic	Amma	CS	$CaSO_4$	16,382

The cement slurry was fully stirred with a water-to-cement ratio of 0.28 and was then poured into a 20 mm × 20 mm × 20 mm mold. The cement slurry specimens were demolded after curing with a temperature of 20 ± 1 °C and 99% relative humidity after 24 h. They were then cured for a standard time of 1, 3 and 28d to test the compressive strength [27].

3. Results and Discussion

3.1. Decomposition Rate of $CaSO_4$ to Free-CaO

The decomposition of $CaSO_4$ determines the actual CaO content participating in the reactions. In addition, the decomposition of $CaSO_4$ has a great influence on the phase formation, phase composition, and even the chemical composition of the mineral phases according to the study of [14,17]. However, the decomposition of $CaSO_4$ to CaO is affected by its proportion in the raw mixture [20]. Thus, it is necessary to confirm the decomposition rate after the calcination. Figure 1 shows the quantitative and theoretical sulfate loss of the clinkers with different CaO sources produced at 1300 °C. As shown in Figure 1, although the same ye'elimite content was designed in clinkers, the actual SO_3 content differs in all clinkers. The SO_3 content increased gradually from clinkers S00 to S80, but then decreased in S100.

**Figure 1.** Quantitative and theoretical sulfate loss in the clinker with different CaO sources.

The gypsum decomposition rates of all clinker were lower than the theoretical value except for S00. In S00, all $CaSO_4$ was assumed to participate in the reactions to form ye'elimite. In fact, there was 14.7 wt.% sulfate loss in the clinker, which led to a higher CaO than the stoichiometric value. However, there was no f-CaO observed in the sample, which means that the extra CaO was involved in the reactions. Extra CaO induces phase equilibrium with a greater ferrite phase (with the $CaO/(Al_2O_3 + Fe_2O_3)$ ratio of 2.0) formed

rather than ye'elimite (with the CaO/(Al₂O₃ + Fe₂O₃) ratio of 1.3), because of the higher CaO/(Al₂O₃ + Fe₂O₃) ratio [28]. In clinkers S10–S100, the sulfate loss was less than the designed value and resulted in less CaO participating in the reactions, which led to more Fe₂O₃ being incorporated into the ye'elimite [17]. The CaO and SO₃ content of the clinkers and the differences between the quantitative and theoretical values are listed in Table 3. The differences caused by different proportions of CaCO₃/CaSO₄ affected the formation of the mineral phases.

Table 3. CaO and SO₃ content of clinkers and their differences between quantitative and theoretical values.

CaO/SO ₃ (Δ) Content	Theo.	S00	S10	S20	S50	S80	S100
SO ₃	6.56	5.58	8.58	10.08	12.01	12.93	8.96
Δ(SO ₃) = S(SO ₃) – Theo.(SO ₃)	–	–0.98	2.02	3.52	5.46	6.37	2.40
CaO	42.53	43.22	41.12	40.07	38.71	38.07	40.85
Δ(CaO) = S(CaO) – Theo.(CaO)	–	0.69	–1.41	–2.46	–3.82	–4.46	–1.68

The actual CaO content involved in the reactions is calculated as in Equation (16). CaCO₃ was assumed to decompose completely above 900 °C and to participate in all reactions. CaO from CaSO₄ was calculated due to the SO₃ content.

$$\text{CaO} = \text{CaCO}_3 \times \frac{M_{\text{CaO}}}{M_{\text{CaCO}_3}} + \left(\text{CaSO}_4 \times \frac{M_{\text{CaO}}}{M_{\text{CaSO}_4}} - \text{SO}_3 \times \frac{M_{\text{CaSO}_4}}{M_{\text{SO}_3}} \times \frac{M_{\text{CaO}}}{M_{\text{CaSO}_4}} \right) \quad (16)$$

3.2. Mineralogical Characterization

3.2.1. Qualitative Phase Analysis

The XRD patterns of the IR-CSA clinker are shown in Figure 2. The key mineral phases, such as ye'elimite and belite existed in all the clinkers, while anhydrite and brownmillerite were partially present. The characteristic peak of anhydrite only presented in clinker S10–S80 and became stronger gradually, which is consistent with the SO₃ content as tested in Section 3.1. The characteristic peak of brownmillerite (around 12.1°) in S00 is the strongest and becomes weaker gradually with the increase in CaSO₄ as a CaO source. The characteristic peak of brownmillerite (around 12.1°) vanished in S50 and S80, but its intensity increased slightly in S100. On one hand, more CaSO₄ batching in the raw material is beneficial for Al₂O₃ to form ye'elimite rather than brownmillerite. With the increase in CaSO₄ as the CaO source, more CaO or CA is wrapped by CaSO₄ so that the formation paths of ye'elimite expressed as Equations (1)–(3) are prior to that of the ferrite phase expressed as Equations (7)–(11). On the other hand, the residual CaSO₄ in the clinker means the low CaO content participates in the reactions, and this induces more Fe₂O₃ to be incorporated into C₄A_{3-x}F_xS̄ than to the form ferrite phase [17].

The characteristic peaks of C₄A₃S̄ and C₂S were also different between the clinkers. The characteristic peak of C₄A₃S̄-*o* (at about 18.1°) was obvious in S00 and became weaker, gradually vanishing when CaSO₄ provided more than 50% CaO. Moreover, the main characteristic peaks of ye'elimite (at approximately 23.7° and 27.4°) gradually shifted to lower angles with the increase in the CaO derived from CaSO₄ (Figure 3a,b). This was mainly because the interplanar spaces of ye'elimite (with the crystal plane exponent of (022) in C₄A₃S̄-*o* and (211) in C₄A₃S̄-*c*, respectively) were increased with the amount of Al³⁺ (0.535 Å) substituted by Fe³⁺ (0.645 Å) [17]. Similarly, the crystal structure of belite was additionally affected by CaO sources and the crystal structure of α'-C₂S was more likely to occur when the CaO source of CaSO₄ was increased (Figure 3c). The most convenient condition for the formation of α'-C₂S is that CaSO₄ provides CaO with the proportion of 50–80 at.% and with anhydrite residue in the clinker.

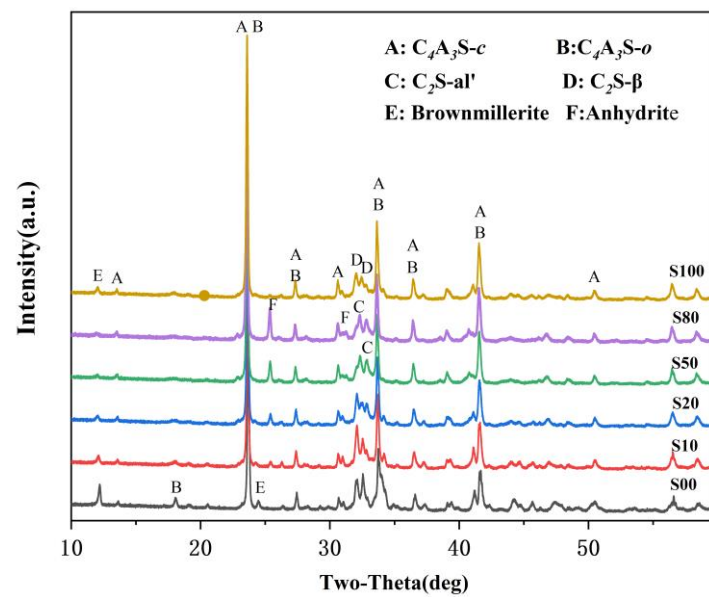


Figure 2. XRD patterns of clinkers S00–S100.

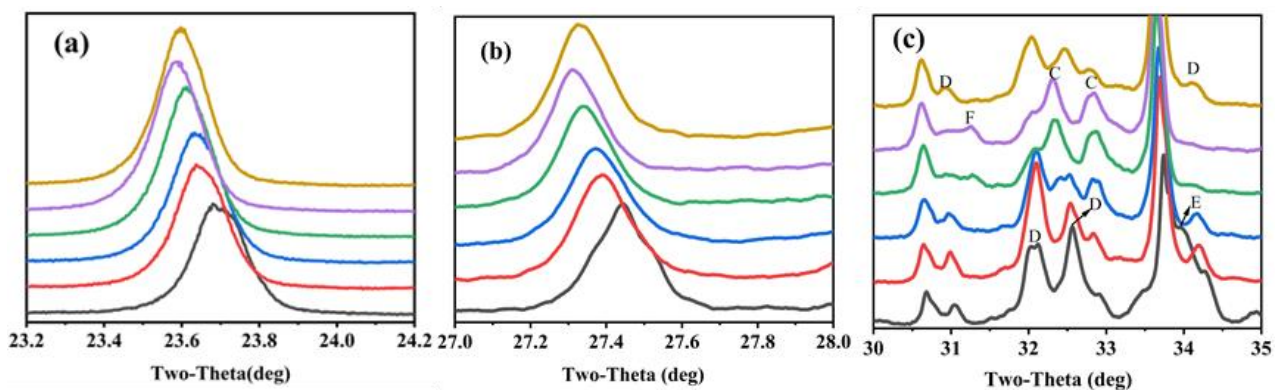


Figure 3. Zoomed section of characteristic peaks migrate with variation proportion of CaSO_4 as a CaO source (a) ye'elimite at about 23.7° , (b) ye'elimite at about 27.4° and (c) belite- α' (C), belite- β (D), brownmillerite (E) and anhydrite (F).

3.2.2. Quantitative Phase Analysis

Quantitative analysis was conducted using the Rietveld refinement to better understand the formation and transformation of the key mineral phases affected by CaO sources. The results (Figure 4) indicate that the $\text{C}_4\text{A}_3\bar{\text{S}}\text{-o}$ decreased while the $\text{C}_4\text{A}_3\bar{\text{S}}\text{-c}$ increased with the increase in CaSO_4 as a CaO source, which indicates that more Fe_2O_3 is incorporated into $\text{C}_4\text{A}_{3-x}\text{F}_x\bar{\text{S}}$ to stabilize $\text{C}_4\text{A}_3\bar{\text{S}}$ as a pseudocubic crystal during the cooling process [29,30]. The crystal types of belite were also affected by CaO sources. The results indicate that C_2S only existed as a beta crystal type in S00; $\beta\text{-C}_2\text{S}$ subsequently decreased gradually from S00 to S80, but increased in S100. However, the $\alpha'\text{-C}_2\text{S}$ phase showed the opposite trend. The literature has reported that the crystal structure of C_2S is correlated to its formation paths and that C_2S as obtained from Equations (5) and (6) exists as $\beta\text{-C}_2\text{S}$, while from Equation (10) as $\alpha'\text{-C}_2\text{S}$ [15]. It is clear that the increasing content of CaSO_4 induces a greater $4\text{CaO}\cdot 2\text{SiO}_2\cdot \text{CaSO}_4$ formation as the transition phase and finally decomposes as $\alpha'\text{-C}_2\text{S}$.

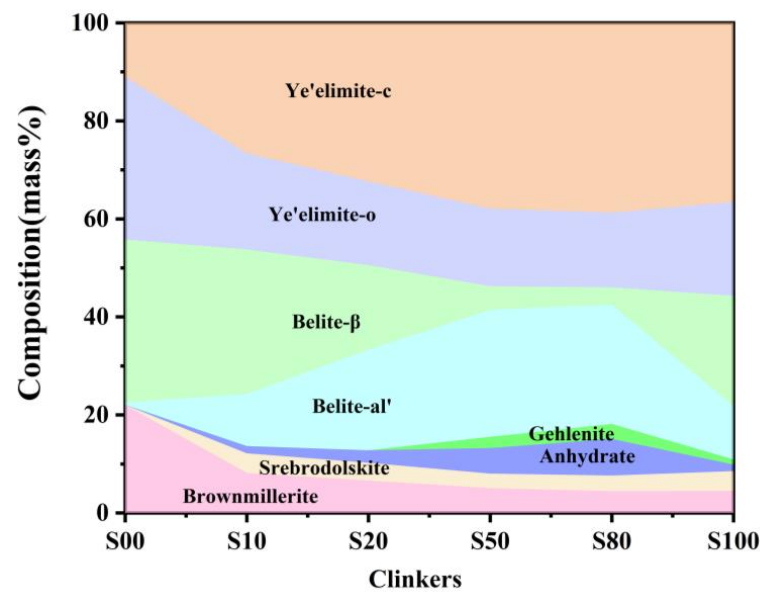


Figure 4. Phase evolution of clinkers S00–S100.

The ferrite phase usually refers to a solid solution with the chemical composition of the formula $\text{Ca}_2(\text{Al}_y\text{Fe}_{2-y})\text{O}_5$, where y can vary from 0 to $4/3$. The ferrite phase, with a chemical composition of $y = 0$, is specified as srebrodolskite (C_2F), and the set of assemblages with $0 < y < 4/3$ usually have a chemical composition approximating to brownmillerite (C_4AF) [17]. The formation of brownmillerite is considered to comprise a continuous solid solution of calcium aluminate with srebrodolskite (C_2F) [31]. In this study, both srebrodolskite and brownmillerite existed in all clinker except for S00. There was no srebrodolskite in clinker S00, which shows that srebrodolskite reacts with calcium aluminate to form brownmillerite. In addition, the content of brownmillerite is slightly higher than the designed value; the main reason for this is that the CaSO_4 is insufficient to react with CA to form $\text{C}_4\text{A}_3\bar{\text{S}}$ due to the partial decomposition, and more CA will be a solid soluble in brownmillerite according to Equations (11) and (12). The content of brownmillerite decreases gradually with the increase in CaSO_4 , as the CaO source. In addition, the brownmillerite is much lower than the designed value in the clinker when CaSO_4 provides the CaO . Small amounts of srebrodolskite were present in clinker S10–S100, which shows that CA is more likely to act with CaSO_4 than C_2F when CaSO_4 batches in raw material as the CaO source.

3.3. Chemical Composition of Key Mineral Phases in Iron-Rich Sulfoaluminate Clinker

The crystal type of ye'elimite is determined by the incorporation level of Fe_2O_3 , and be'lite is affected by the incorporation of SO_3 and Fe_2O_3 , to inhibit crystal transformation during cooling. It is clear that the chemical composition of the mineral phase is affected by the CaO source, in accordance with the results specified in Section 3.2, and this could be determined by the elemental distribution obtained from the polished sections of the sample slices by EPMA; the results are shown in Figure 5 (back-scattered electron (BSE) micrograph Figure 5a—S00, Figure 5b—S50, Figure 5c—S80, Figure 5d—S100) and Figure 6 (a: with the back-scattered electron (BSE) micrograph; b element distribution map). There are 300×225 quantitative points of the polished area with elements as shown on the map.

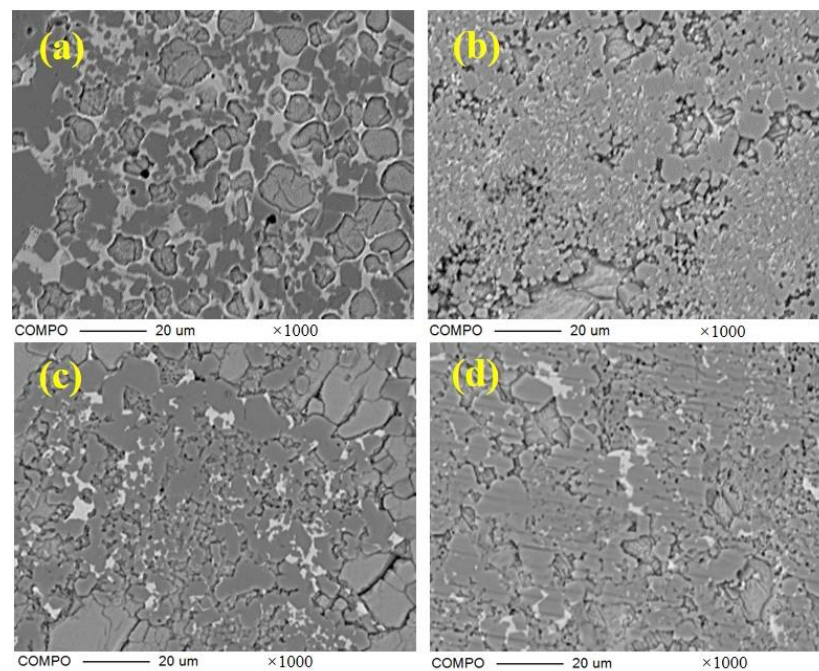


Figure 5. BSE micrograph of polished section of samples with 1000 times magnification; (a) S00; (b) S50; (c) S80; (d) S100.

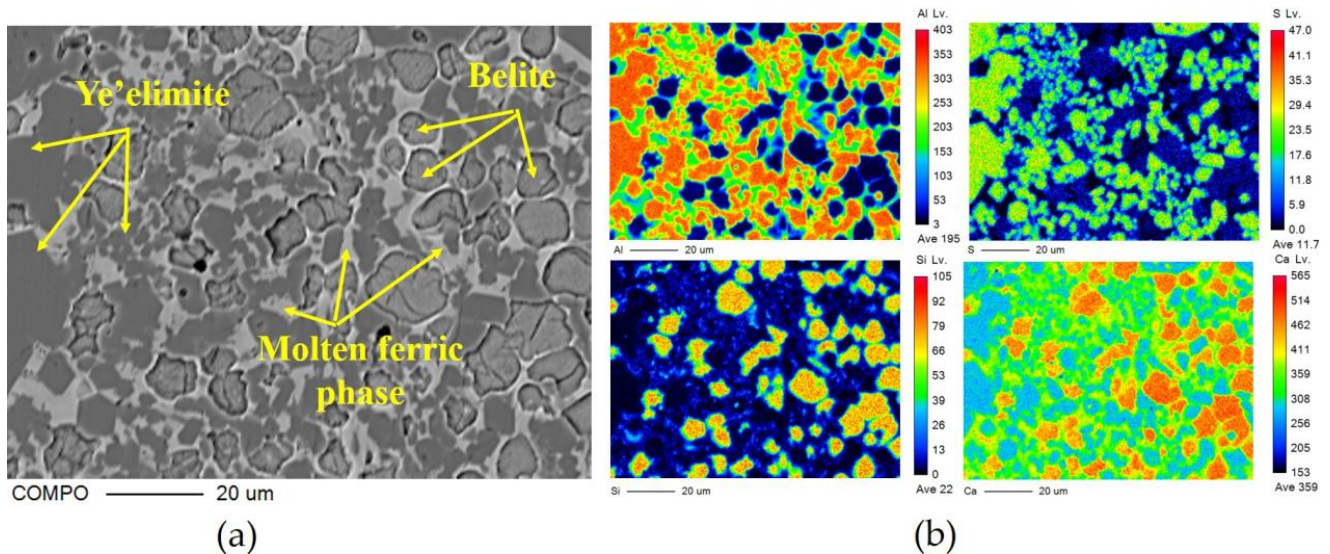


Figure 6. EPMA results of clinker S00: (a) BSE micrograph of polished section; (b) distribution of all measured elements (Al, S, Si and Ca).

3.3.1. Chemical Composition of Ye'Elimite

To obtain the chemical composition of ye'elimite, element contents were sorted and calculated from the ye'elimite phase area. The elemental composition of oxygen atoms was normalized to 16 for comparison. The results are presented in Table 4. The Al^{3+} is substituted by Fe^{3+} in all clinkers; however, the substitution rate was influenced by the CaO source. The content of Al^{3+} substituted by Fe^{3+} was much lower in clinker S00 than the other three. The maximum substitution rate of Fe^{3+} for Al^{3+} reached 17.34 wt.% in clinker S80, and the maximum proportion of Fe_2O_3 in the ye'elimite phase was 6.89 wt.%, expressed as $\text{C}_4\text{A}_{2.71}\text{F}_{0.29}\bar{\text{S}}$.

Table 4. Mineralogical composition of ye'elimite phase of samples S00, S50, S80 and S100.

Sample	Mineralogical Composition	Fe/(Al + Fe)(wt.%)	Fe ₂ O ₃ in Ye'elimite Phase(wt.%)
S00	Ca _{4.0} Al _{5.82} Fe _{0.17} Si _{0.07} S _{0.96} O ₁₆	5.71	2.19
S50	Ca _{3.94} Al _{5.17} Fe _{0.45} Si _{0.13} S _{1.08} O ₁₆	15.29	4.91
S80	Ca _{3.93} Al _{5.24} Fe _{0.53} Si _{0.13} S _{1.12} O ₁₆	17.34	6.89
S100	Ca _{4.06} Al _{5.09} Fe _{0.46} Si _{0.14} S _{1.12} O ₁₆	15.79	6.03

3.3.2. Chemical Composition of Belite

The same method was used to study the chemical composition of the belite phase as was used for ye'elimite. The elemental composition of the belite phase area was calculated and oxygen atoms were normalized to four for comparison. The chemical composition of the belite phase is presented in Table 5. The result indicates that the amount of Fe₂O₃ solidified into belite was much lower than that in C₄A₃S̄; the maximum value reached 1.86 wt.% in clinker S00. The main reason may be that Fe³⁺ is easier to substitute than Al³⁺ in C₄A₃S̄ due to the same valence state and similar ionic radius rather than entering the lattice gap of C₂S.

Table 5. Mineralogical composition of belite phase of samples S00, S50, S80 and S100.

Sample	Mineralogical Composition	Fe ₂ O ₃ in Belite Phase (wt.%)	SO ₃ in Belite Phase (wt.%)
S00	Ca _{1.97} Al _{0.08} Fe _{0.04} Si _{0.85} S _{0.05} O ₄	1.86	2.32
S50	Ca _{1.96} Al _{0.01} Fe _{0.02} Si _{0.81} S _{0.12} O ₄	0.93	5.56
S80	Ca _{1.92} Al _{0.01} Fe _{0.01} Si _{0.91} S _{0.11} O ₄	0.47	5.58
S100	Ca _{1.87} Al _{0.05} Fe _{0.02} Si _{0.84} S _{0.14} O ₄	0.93	4.65

SO₃ was also incorporated into C₂S, and the incorporated amount increased with the increasing content of CaSO₄ as the CaO sources in the raw mixture until 80%, and then decreased slightly when CaO was entirely sourced from CaSO₄. The maximum incorporation content of SO₃ reached 5.58 wt.% in clinker S80 but was 4.65 wt.% in clinker S100. It is worth noting that the crystal type of belite is closely related to the SO₃ content incorporated into the C₂S. Usually, belite exists as α'-C₂S at 830–1470 °C and transforms to β-C₂S at temperatures between 520 °C and 670 °C. Finally, it transforms to γ-C₂S below 520 °C. However, the crystal transformation of C₂S can slow down or even not occur under the influence of CaSO₄. In addition, C₂S obtained from Equations (5) and (6) exists as β-C₂S but as α'-C₂S from Equation (10) according to [15]. In clinker S00, the CaSO₄ is exhausted after reacting with calcium aluminate or gehlenite to form ye'elimite that no more CaSO₄ exist and the reactions of Equations (9) and (10) will not happen. Thus, the belite in clinker S00 exists as β-C₂S. It is obvious that the increasing CaSO₄ content induces more 4CaO·2SiO₂·CaSO₄ formed as a transition phase and finally decomposed as α'-C₂S [15]. Therefore, more α'-C₂S is formed at the expense of β-C₂S with the increase in CaSO₄ as a CaO source. However, the decomposition of CaSO₄ in S100 may be faster than in the others and CaSO₄ rarely exists in the clinker. The reactions of Equations (9) and (10) are hampered, and the proportion of α'-C₂S decreases with the increased CaSO₄ in the raw mixture.

3.3.3. Chemical Composition of Ferrite Phase

The ferrite phase is a solid solution that mainly contains C₂F, C₆AF₂, C₄AF, and C₆A₂F. It is generally believed that iron is distributed in the CSA clinker in the form of C₄AF but mainly exists as C₆AF₂ in the IR-CSA clinker. Iron distributed in the ferrite phase is presented in Figure 7 and the EPMA confirms its inhomogeneous distribution. Iron decreased from the center to the edge in all clinkers, which is consistent with the results of [14]. The ferrite phase is uniformly dispersed around the ye'elimite in clinker S00 and S50, but is concentrated in several areas as small clumps in S80 and S100. The content

of the ferrite phase decreased with the increase in CaSO_4 as the CaO source. To obtain the chemical composition of the ferrite phase, oxygen atoms were normalized to 15 for comparison. The results (presented in Table 6) indicate that the chemical composition in the ferrite phase is close to C_4AF in S00 and S50 but close to C_6AF_2 in clinker S80 and S100. Although there is less iron in the form of the ferrite phase because of the incorporation into ye'elinite in clinkers S80 and S100 than in clinkers S00 and S50, CA is more likely to combine with CaSO_4 Equation (3) than C_2F Equation (8) or C_6AF_2 Equation (11) with the increasing CaSO_4 content in the raw mixture. Thus, the ferrite phase in clinkers S80 and S100 has a chemical composition with lower aluminum but higher iron content than in clinkers S00 and S50.

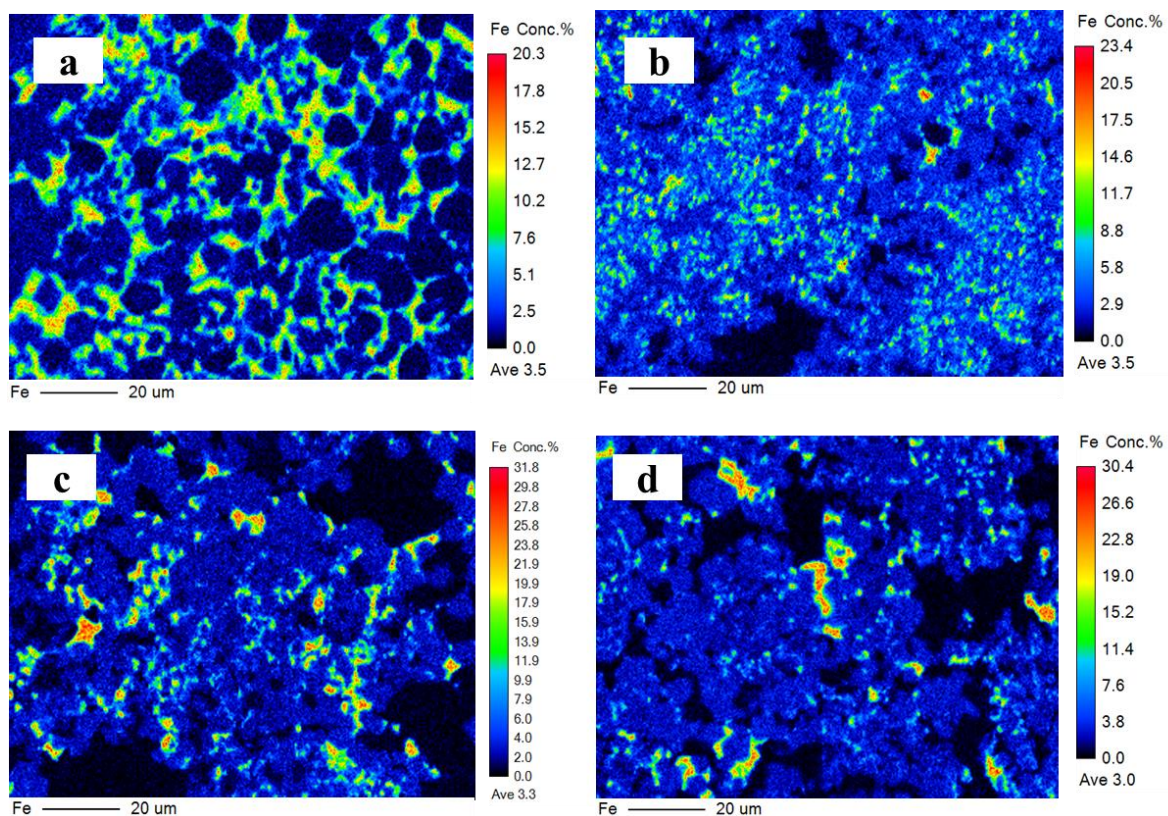


Figure 7. Iron distribution on polished surface of clinker S00 (a), S50 (b), S80 (c), and S100 (d).

Table 6. Chemical composition of ferrite phase of samples S00, S50, S80, and S100.

Sample	Chemical Composition	Fe/Al	Abbreviations
S00	$\text{Ca}_{6.31}\text{Al}_{2.98}\text{Fe}_{2.82}\text{O}_{15}$	0.95	$\text{C}_{4.23}\text{AF}_{0.95}$
S50	$\text{Ca}_{6.32}\text{Al}_{2.68}\text{Fe}_{2.98}\text{O}_{15}$	1.12	$\text{C}_{4.71}\text{AF}_{1.12}$
S80	$\text{Ca}_{6.46}\text{Al}_{1.92}\text{Fe}_{3.77}\text{O}_{15}$	1.96	$\text{C}_{6.73}\text{AF}_{1.96}$
S100	$\text{Ca}_{6.47}\text{Al}_{1.82}\text{Fe}_{3.87}\text{O}_{15}$	2.12	$\text{C}_{7.11}\text{AF}_{2.12}$

3.4. Microstructural Characterization

Figure 8 shows the scanning electron micrograph of the section of the clinker sintered at $1300\text{ }^\circ\text{C}$ for 45 min. All samples are magnified 5000 times. The hexagonal platy structure or quadrilateral columnar structure can be seen, and the particle size of $\text{C}_4\text{A}_{3-x}\text{F}_x\bar{\text{S}}$ in S00 is about $10\text{ }\mu\text{m}$, decreasing drastically in clinker S10 and then increasing gradually in S100. The iron-rich molten phase can be seen clearly around the ye'elinite in S00, which indicates a large amount of liquid ferrite phase during the process. However, the molten phase could hardly be observed in any other clinker with CaSO_4 as the CaO source.

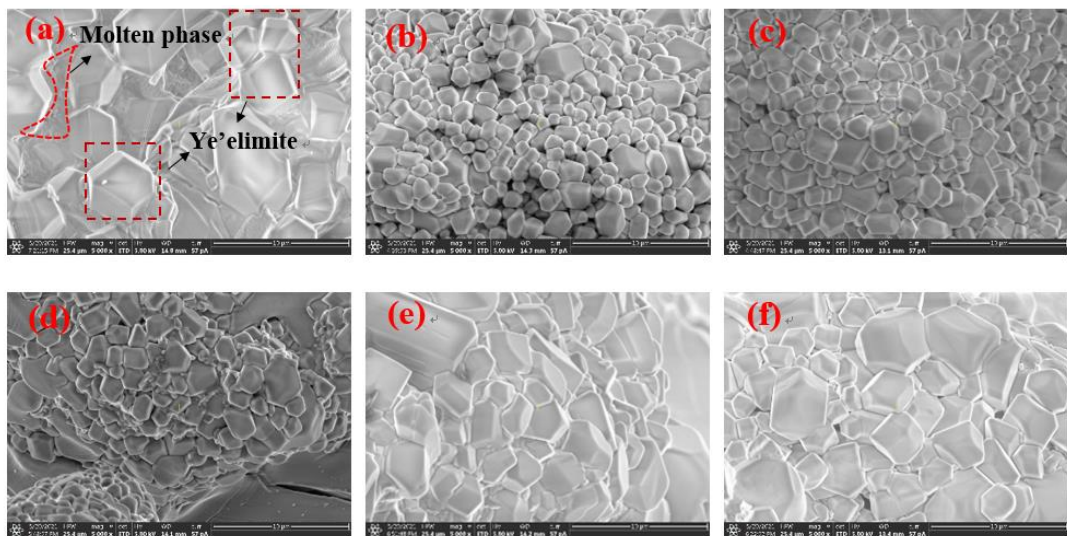


Figure 8. Scanning electron micrograph of section of clinkers S00 (a), S10 (b), S20 (c), S50 (d), S80 (e) and S100 (f).

3.5. Compressive Strength of the IR-CSA Cement

The compressive strength of IR-CSA cement clinkers S00–S100 after 1 d, 3 d, and 28 d of curing is shown in Figure 9. With the increase in CaO derived from CaSO₄, the 1 d and 3 d compressive strength exhibited slight strength advantages in cements S50 and S80, but disadvantages in S100. The 28d compressive strength was higher for cement S50–S100 than for S00–S20. To be specific, the cement in S50 showed the best early and late compressive strength. The main reasons may be as follows: (i) The anhydrate in cements S50 and S80 consumes more water for ye'elimite hydration than gypsum according to Equation (14); thus, the actual water/cement ratios of cements S50 and S80 were lower than other samples, affecting their mechanical properties; (ii) The Al/Fe ratio of the ferrite phase of S50 (1:1.12) was higher than S80 (1:1.96) and S100 (1:2.12), which resulted in higher hydration activity of the ferrite phase and early compressive strength of the S50 than the S80 and S100. Furthermore, the $C_4A_{3-x}F_x\bar{S}$ particle size of S50 was smaller than S80 and S100, which was beneficial for the hydration rate and early compressive strength; (iii) The late compressive strength was related to the hydration of $C_4A_{3-x}F_x\bar{S}$ and C_2S . With the increase in CaSO₄ as a CaO source, the content of $C_4A_{3-x}F_x\bar{S}$ in clinkers S50–S100 was higher than in S00–S20. In addition, the C_2S hydration activity in S50 and S80 is higher than in the other cements because of the crystal type (the crystal type of α' - C_2S exhibits higher hydration activity than β - C_2S at room temperature).

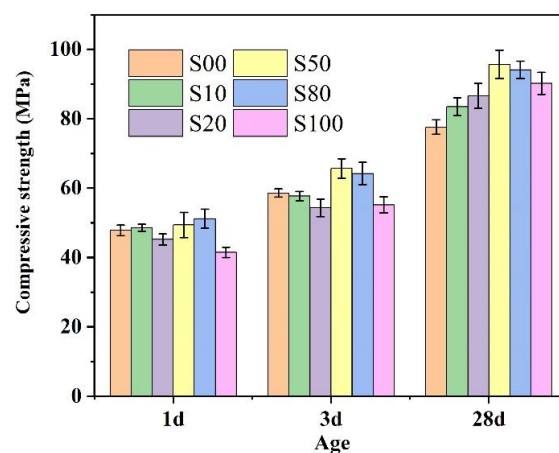


Figure 9. Compressive strength of cements S00–S100.

4. Conclusions

The effect of CaO sources, from either CaCO_3 or CaSO_4 , on phase formation and mineral composition of iron-rich clinker was investigated by varying their proportions in raw materials. Compared with CaCO_3 , CaO derived from CaSO_4 was more conducive for Al_2O_3 and Fe_2O_3 to form $\text{C}_4\text{A}_{3-x}\text{F}_x\bar{\text{S}}$ rather than the ferrite phase which resulted in an increased content of ye'elimite but a decreased ferrite phase. More c- $\text{C}_4\text{A}_{3-x}\text{F}_x\bar{\text{S}}$ formed at the expense of o- $\text{C}_4\text{A}_{3-x}\text{F}_x\bar{\text{S}}$ in the clinker because of the incorporation of Fe_2O_3 . In addition, the belite phase was more inclined to exhibit as α' - C_2S instead of β - C_2S when taking CaSO_4 as a CaO source, which is conducive to the hydration activity of the clinker. Finally, the crystal grain sizes decreased dramatically and then increased gradually with the increase in the proportion of CaO derived from CaSO_4 . In view of the influence of the mineral composition, crystal structure and crystal grain sizes, cement with optimal mechanical properties was obtained with the proportion of 1:1 of CaCO_3 and CaSO_4 as a CaO source.

Under the specified conditions, the substitution of Fe^{3+} for Al^{3+} reached a maximum value of 17.34 wt.%, and the maximum proportion of Fe_2O_3 in the ye'elimite phase was 6.89 wt.%, expressed as $\text{C}_4\text{A}_{2.71}\text{F}_{0.29}\bar{\text{S}}$. However, the incorporation amount of Fe_2O_3 into C_2S was no more than 1.86 wt.% and showed an irregular change trend with CaO sources. The chemical formula of the ferrite phase was calculated and found to be similar to C_4AF when the amount of CaO derived from CaSO_4 was less than 50% but similar to C_6AF_2 when the amount of CaO derived from CaSO_4 was more than 80%, which also indicates that Al_2O_3 is more inclined to be involved in $\text{C}_4\text{A}_{3-x}\text{F}_x\bar{\text{S}}$ with the increase in CaSO_4 as a CaO source.

The findings provide a possible method to optimize the mineral composition of IR-CSA clinker by adjusting the content of CaSO_4 as a CaO source and to produce high-performance IR-CSA cement at a low cost through cooperative utilization of waste gypsum and iron-bearing industrial solid wastes.

Author Contributions: Methodology, Writing—original draft, Data Curation, W.J.; writing—review and editing, C.W. and C.Z.; Project administration, X.W. and J.L.; Investigation, S.W. and Y.Y.; Formal analysis, Y.L. and W.W.; Conceptualization, resources, project administration. All authors have read and agreed to the published version of the manuscript.

Funding: This work was funded by the National Key Research and Development Program of China (No.2020YFC191000) and the Key Research and Development Program of Shandong Province-Major Scientific and Technological Innovation Project (No.2020 CXGC011403).

Institutional Review Board Statement: Not applicable.

Informed Consent Statement: Not applicable.

Data Availability Statement: The data presented in this study are available on request from the corresponding author.

Conflicts of Interest: No conflict of interest exists in the submission of this manuscript, and the manuscript was approved by all authors for publication. I would like to declare on behalf of my co-authors that the work described was original research that has not been published previously, and is not under consideration for publication elsewhere, in whole or in part. All the authors listed have approved the manuscript that is enclosed.

References

1. Sharp, J.H. Calcium sulfoaluminate cements—Low-energy cements, special cements or what? *Adv. Cem. Res.* **1999**, *11*, 3–13. [[CrossRef](#)]
2. Zhang, L.; Su, M.; Wang, Y. Development of the use of sulfo- and ferroaluminate cements in China. *Adv. Cem. Res.* **1999**, *11*, 15–21. [[CrossRef](#)]
3. Haha, M.B.; Winnefeld, F.; Pisch, A. Advances in understanding ye'elimite-rich cements. *Cem. Concr. Res.* **2019**, *123*, 105778. [[CrossRef](#)]
4. Singh, M.; Upadhyay, S.; Prasad, P. Preparation of iron rich cements using red mud. *Cem. Concr. Res.* **1997**, *27*, 1037–1046. [[CrossRef](#)]

5. Khalil, N.; Aouad, G.; El Cheikh, K.; Rémond, S. Use of calcium sulfoaluminate cements for setting control of 3D-printing mortars. *Constr. Build. Mater.* **2017**, *157*, 382–391. [[CrossRef](#)]
6. Péra, J.; Ambroise, J. New applications of calcium sulfoaluminate cement. *Cem. Concr. Res.* **2004**, *34*, 671–676. [[CrossRef](#)]
7. Mao, Y.; Wu, H.; Wang, W.; Jia, M.; Che, X. Pretreatment of municipal solid waste incineration fly ash and preparation of solid waste source sulfoaluminate cementitious material. *J. Hazard Mater.* **2020**, *385*, 121580. [[CrossRef](#)]
8. Zhang, C.; Wang, G.; Wu, C.; Li, J.; Wu, S.; Jiang, W.; Wang, X.; Wang, W.; Feng, M. Investigation of hierarchical porous cold bonded lightweight aggregates produced from red mud and solid-waste-based cementitious material. *Constr. Build. Mater.* **2021**, *308*, 124990. [[CrossRef](#)]
9. Ge, Z.; Yuan, H.; Sun, R.; Zhang, H.; Wang, W.; Qi, H. Use of green calcium sulfoaluminate cement to prepare foamed concrete for road embankment: A feasibility study. *Constr. Build. Mater.* **2020**, *237*, 117791. [[CrossRef](#)]
10. Álvarez-Pinazo, G.; Santacruz, I.; León-Reina, L.; Aranda, M.A.G.; De la Torre, A.G. Hydration Reactions and Mechanical Strength Developments of Iron-Rich Sulfoaluminate Eco-cements. *Ind. Eng. Chem. Res.* **2013**, *52*, 16606–16614. [[CrossRef](#)]
11. Bullerjahn, F.; Scholten, T.; Scrivener, K.L.; Ben Haha, M.; Wolter, A. Formation, composition and stability of ye'elimite and iron-bearing solid solutions. *Cem. Concr. Res.* **2020**, *131*, 106009. [[CrossRef](#)]
12. Idrissi, M.; Diouri, A.; Damidot, D.; Greneche, J.M.; Talbi, M.A.; Taibi, M. Characterisation of iron inclusion during the formation of calcium sulfoaluminate phase. *Cem. Concr. Res.* **2010**, *40*, 1314–1319. [[CrossRef](#)]
13. Guo, Y.; Su, M.; Deng, J.; Wang, Y. A study on hydration characteristics of ferrite phase in ferro aluminate cement. *J. Chin. Chem. Soc.* **1989**, *17*, 296–301.
14. Wu, S.; Yao, X.; Ren, C.; Yao, Y.; Zhang, C.; Wu, C.; Wang, W. Effect of iron on the preparation of iron-rich calcium sulfoaluminate cement using gypsum as the sole calcium oxide source and its incorporation into mineral phases. *Constr. Build. Mater.* **2021**, *290*, 123214. [[CrossRef](#)]
15. Wang, Y.; Su, M.; Zhang, L. *Sulfoaluminate Cement*; Beijing University of Technology Press: Beijing, China, 1999.
16. Chen, D.; Feng, X.; Long, S. The influence of ferric oxide on the properties of $3\text{CaO} \cdot 3\text{Al}_2\text{O}_3 \cdot \text{CaSO}_4$. *Thermochim. Acta* **1993**, *215*, 157–169. [[CrossRef](#)]
17. Yao, X.; Yang, S.; Dong, H.; Wu, S.; Liang, X.; Wang, W. Effect of CaO content in raw material on the mineral composition of ferric-rich 1 sulfoaluminate clinker. *Constr. Build. Mater.* **2020**, *263*, 120431. [[CrossRef](#)]
18. Huang, Y.; Pei, Y.; Qian, J.; Gao, X.; Liang, J.; Duan, G.; Zhao, P.; Lu, L.; Cheng, X. Bauxite free iron rich calcium sulfoaluminate cement: Preparation, hydration and properties. *Constr. Build. Mater.* **2020**, *249*, 118774. [[CrossRef](#)]
19. Bullerjahn, F.; Schmitt, D.; Ben Haha, M. Effect of raw mix design and of clinking process on the formation and mineralogical composition of (ternesite) belite calcium sulfoaluminate ferrite clinker. *Cem. Concr. Res.* **2014**, *59*, 87–95. [[CrossRef](#)]
20. Yao, X.; Yang, S.; Huang, Y.; Wu, S.; Yao, Y.; Wang, W. Effect of CaSO_4 batching in raw material on the iron-bearing mineral transition of ferric-rich sulfoaluminate cement. *Constr. Build. Mater.* **2020**, *250*, 118783. [[CrossRef](#)]
21. Ren, C.; Wang, W.; Li, G. Preparation of high-performance cementitious materials from industrial solid waste. *Constr. Build. Mater.* **2017**, *152*, 39–47. [[CrossRef](#)]
22. Liu, N.; Chen, Q.; Dang, Y.; Li, F.; Zhang, J.; Li, X.; Qian, J. Partial Decomposition of Phosphogypsum for the Preparation of Belite Calcium Sulfoaluminate Cement. *Bull. Chin. Ceram. Soc.* **2016**, *35*, 3763–3769.
23. Wu, S.; Yao, X.; Ren, C.; Li, J.; Xu, D.; Wang, W. Co-preparation of calcium sulfoaluminate cement and sulfuric acid through mass utilization of industrial by-product gypsum. *J. Clean. Prod.* **2020**, *265*, 121801. [[CrossRef](#)]
24. Jeong, Y.; Hargis, C.; Chun, S.; Moon, J. The effect of water and gypsum content on strätlingite formation in calcium sulfoaluminate-belite cement pastes. *Constr. Build. Mater.* **2018**, *166*, 712–722. [[CrossRef](#)]
25. García-Maté, M.; De la Torre, A.G.; León-Reina, L.; Losilla, E.R.; Aranda, M.A.G.; Santacruz, I. Effect of calcium sulfate source on the hydration of calcium sulfoaluminate eco-cement. *Cem. Concr. Compos.* **2015**, *55*, 53–61. [[CrossRef](#)]
26. Coelho, A.A. TOPAS and TOPAS-Academic: An optimization program integrating computer algebra and crystallographic objects written in C++. *J. Appl. Crystallogr.* **2018**, *51*, 210–218. [[CrossRef](#)]
27. Yao, Y.; Wang, W.; Ge, Z.; Ren, C.; Yao, X.; Wu, S. Hydration study and characteristic analysis of a sulfoaluminate high-performance cementitious material made with industrial solid wastes. *Cem. Concr. Compos.* **2020**, *112*, 103687. [[CrossRef](#)]
28. Touzo, B.; Scrivener, K.L.; Glasser, F.P. Phase compositions and equilibria in the $\text{CaO}-\text{Al}_2\text{O}_3-\text{Fe}_2\text{O}_3-\text{SO}_3$ system, for assemblages containing ye'elimite and ferrite $\text{Ca}_2(\text{Al,Fe})\text{O}_5$. *Cem. Concr. Res.* **2013**, *54*, 77–86. [[CrossRef](#)]
29. Ndzila, J.S.; Liu, S.; Jing, G.; Wang, S.; Ye, Z. The effect of Fe^{3+} ion substitution on the crystal structure of ye'elimite. *Ceram. Silik.* **2020**, *64*, 18–28. [[CrossRef](#)]
30. Huang, Y.; Shen, X.; Ma, S.; Chen, L.; Zhong, B. Effect of Fe_2O_3 on the formation of calcium sulphaluminate mineral. *J. Chin. Ceram. Soc.* **2007**, *35*, 485–488.
31. Guo, Y.; Deng, J.; Su, M.; Wang, Y. A study on formation mechanism of ferrite phase in ferroaluminate cement. *J. Chin. Chem. Soc.* **1988**, *16*, 481–488.

Disclaimer/Publisher's Note: The statements, opinions and data contained in all publications are solely those of the individual author(s) and contributor(s) and not of MDPI and/or the editor(s). MDPI and/or the editor(s) disclaim responsibility for any injury to people or property resulting from any ideas, methods, instructions or products referred to in the content.